Mineralogical Magazine, December 2005, Vol. 69(6), pp. 1047–1057

Aspidolite, the Na analogue of phlogopite, from Kasuga-mura, Gifu Prefecture, central Japan: description and structural data

Y. BANNO[1,*], R. MIYAWAKI[2], T. KOGURE[3], S. MATSUBARA[2], T. KAMIYA[4] AND S. YAMADA[5]

[1] Geological Survey of Japan, National Institute of Advanced Industrial Science and Technology (AIST), 1-1-1 Higashi, Tsukuba, Ibaraki, 305-8567, Japan
[2] Department of Geology, The National Science Museum, 3-23-1 Hyakunin-cho, Shinjuku-ku, Tokyo, 169-0073, Japan
[3] Department of Earth and Planetary Science, Graduate School of Science, The University of Tokyo, 7-3-1 Hongo, Bunkyo-ku, Tokyo, 113-0033, Japan
[4] Tsukaguchihon-machi, Amagasaki, Hyogo, 661-0001, Japan
[5] 92 Hoshino, Kiyomizu, Higashiyama, Kyoto, 605-0853, Japan

ABSTRACT

Aspidolite, the Na analogue of phlogopite, ideally $NaMg_3AlSi_3O_{10}(OH)_2$, occurring in hornfels from a contact aureole in Kasuga-mura, central Japan, has been approved as a mica species by the Commission on New Minerals and Mineral Names of the International Mineralogical Association. Aspidolite is interleaved with and surrounded by phlogopite. Based on its mode of occurrence, phlogopite is classified into two types; (1) phlogopite interleaved with aspidolite (= interleaved phlogopite) and (2) phlogopite rim. The aspidolite-phlogopite assemblage is associated with amphibole (pargasite-magnesiosadanagaite), titanite, calcite, scapolite, apatite, pyrrhotite and chalcopyrite. A representative chemical formula of aspidolite is $(Na_{0.90}K_{0.10})_{\Sigma 1.00}(Mg_{2.27}Al_{0.41}Fe^{2+}_{0.23}Ti_{0.05})_{\Sigma 2.96}(Al_{1.44}Si_{2.56})_{\Sigma 4.00}O_{10}(OH_{1.97}F_{0.03})_{\Sigma 2.00}$. Aspidolite has almost fully occupied the interlayer site; its Na/(Na+K) ratio ranges from 0.67 to 0.95. It has more tetrahedral Al (1.38–1.48 a.p.f.u. for O = 11) than the ideal aspidolite end-member showing progression of tschermakite-type substitution. The alternation of aspidolite and phlogopite parallel to the (001) plane may indicate a miscibility gap between these two phases. The phlogopite rim is interpreted as a later product, probably formed metasomatically. Aspidolite is optically biaxial negative with elongation positive and $Z \parallel$ cleavage. Two polytypes (1*M* and 1*A*) of aspidolite were identified in X-ray powder diffraction patterns. Aspidolite-1*M* is monoclinic, space group *C*2/*m*, with refined unit-cell parameters a = 5.291(8), b = 9.16(2), c = 10.12(2) Å, β = 105.1(1)°, V = 473(1) Å^3, Z = 2. Aspidolite-1*A* is triclinic, space group $C\bar{1}$, with a = 5.289(6), b = 9.16(1), c = 9.892(9) Å, α = 94.45(9), β = 97.74(9), γ = 90.0(1)°, V = 473.4(9) Å^3, Z = 2.

KEYWORDS: aspidolite, new mineral species, sodium mica, phlogopite, trioctahedral mica, X-ray powder diffraction data, Kasuga-mura, Japan.

Introduction

ASPIDOLITE, first found in chlorite schists from Zillertal, Austria, was initially defined by von Kobell (1869) as a Na- and Mg-dominant mica belonging to the biotite–phlogopite series, which was later interpreted as the Na-dominant analogue of phlogopite (Franz and Althaus, 1976). Schreyer *et al*. (1980) described the Na analogue of phlogopite from a metamorphosed evaporite sequence in Algeria and termed it 'sodium phlogopite'. However, they did not apply for a new mineral species to be approved by the Commission on New Minerals and Mineral Names (CNMMN) of the International Mineralogical Association (IMA). Na phlogopites

* E-mail: y-banno@aist.go.jp
DOI: 10.1180/0026461056960307

were also found in igneous rocks. They occur as inclusions in chromites of mafic layered intrusions (Talkington *et al*., 1986; Lorand and Cottin, 1987) and ophiolite complexes (Augé, 1987; Peng *et al*., 1995; Arai *et al*., 1997; Matsumoto and Arai, 1997; Schiano *et al*., 1997; Tsujimori *et al*., 1998). In 1998, the mica nomenclature was revised by the IMA, and the name aspidolite was resurrected as a formal species name to replace sodium phlogopite (Rieder *et al*., 1998). According to this mica nomenclature, aspidolite was defined as trioctahedral mica with end-member formula $NaMg_3AlSi_3O_{10}(OH)_2$. There are current reports of aspidolite which occurs from norite xenoliths (Costa *et al*., 2001) and ruby-bearing marbles (Garnier *et al*., 2004). Although aspidolite was known for more than a century as probably representing true mica, no detailed mineral descriptions including crystallographic data for the Na analogue of phlogopite were reported. Therefore, the mineral aspidolite has not been formally described as a species until now. Recently, the crystal structure of aspidolite from a contact aureole in Kasuga-mura, central Japan, was investigated by high-resolution transmission electron microscopy (HRTEM) (Kogure *et al*., 2004). They indicated that (1) there is a large layer offset, i.e. lateral shift between two tetrahedral sheets across the Na-bearing interlayer region, and (2) the ordered aspidolite has different one-layer structures with monoclinic ([$\bar{1}$00] layer offset) and triclinic ([110] or [1$\bar{1}$0] layer offset) cells. These monoclinic and triclinic aspidolites are described as aspidolite-1*M* and aspidolite-1*A*, respectively. Further investigation of the aspidolite from the same specimens allowed the approval of the mineral data and mineral name by the CNMMN (no. 2004-049). In this paper, we will present a description of aspidolite from Kasuga-mura. The type specimens of aspidolite have been deposited at the Geological Museum, Geological Survey of Japan, AIST, Tsukuba, under the registered number GSJ M35151-4 and National Science Museum, Tokyo, under the catalogue no. NSM-28719.

Geological setting and petrography

The Kasuga-mura area comprises Jurassic rock and Cretaceous Kaizuki-yama granite. The rock formation of Jurassic age consists of shale, sandstone, and chert with substantial amounts of basic volcanics, dolomite, and limestone. This formation was thermally metamorphosed by the Kaizuki-yama granite. The contact aureole around the Kaizuki-yama granite is >3 km wide, and its metamorphic grade ranges from the greenschist to the amphibolite facies (Fig. 1; Suzuki, 1975, 1977). The contact aureole is divided into four mineral zones on the basis of mineral parageneses

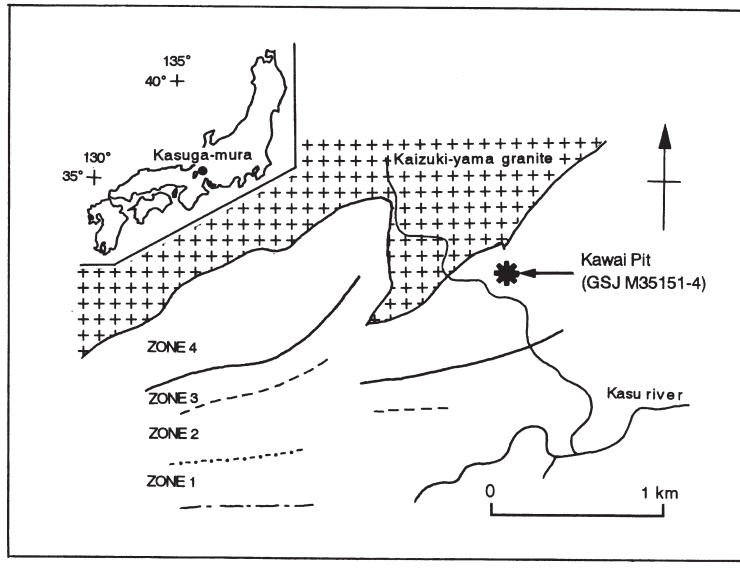

FIG. 1. Schematic geological map of the Kasuga-mura area showing the four metamorphic zones (after Suzuki, 1977). Also shown is the sample locality.

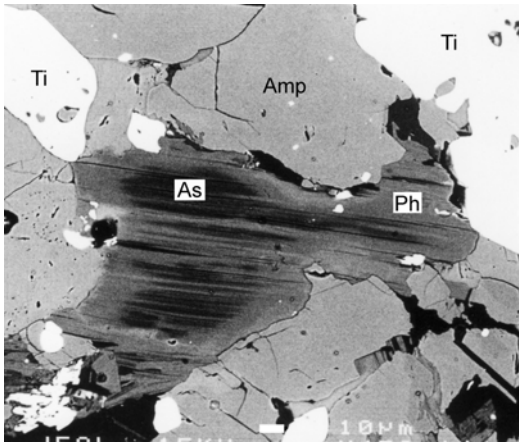

FIG. 2. Back-scattered electron image of aspidolite interleaved with and rimmed by phlogopite. Scale bar is 10 μm. As = aspidolite, Ph = phlogopite, Amp = amphibole, Ti = titanite.

in the siliceous dolomite; zone 1 is defined by the presence of talc, zone 2 by the assemblage dolomite-quartz-tremolite-calcite, zone 3 by the assemblage diopside-dolomite, and zone 4 by the assemblage forsterite-diopside. The aspidolite-bearing sample was collected from waste rock (probably representing zone 4) in the Kawai pit of the Kasuga mine, which had produced wollastonite and dolomite (Fig. 1). The sample is mainly composed of phlogopitic mica, amphibole, titanite, calcite, scapolite, apatite, pyrrhotite and chalcopyrite with minor chlorite and pyrite.

The phlogopitic mica is pale brown and occurs as plates ~0.1–1.2 mm long. In the back-scattered electron image, the mica shows a different zone of brightness mainly due to the variation of K and Na contents (Fig. 2). This image reveals that mica is a composite crystal consisting of aspidolite and phlogopite. Aspidolite is interleaved with and rimmed by phlogopite (Fig. 2). On the mode of occurrence, two types of phlogopite are distinguished; (1) interleaved phlogopite, and (2) phlogopite rim. The interleaved phlogopite is generally parallel to the (001) plane. It is <~70 μm wide. The phlogopite rim is <~50 μm wide.

Amphibole occurs as prismatic crystals, up to 3 mm long. It exhibits distinct optical zoning, with a pargasite core and magnesiosadanagaite rim (Banno *et al*., 2004). The rim is characterized by a pleochroism (yellowish brown to pale yellowish brown) stronger than the core (pale greenish brown to pale brown). Chlorite occurs as flakes in mica crystals, parallel to their (001) plane. In rare cases, chlorite extensively replaces the mica grains. Scapolite occurs as subhedral grains, up to 7 mm in size, and is often replaced by fine-grained muscovite. Titanite and apatite form euhedral to subhedral crystals <0.5 mm long.

Mineral chemistry

Mineral analyses were performed on a JEOL JXA-8800R electron microprobe. Accelerating voltage and specimen current were kept at 15 kV and 12 nA on the Faraday cup, respectively. The beam diameter was 10 μm for the analyses of F and Cl, and 2 μm for the other elements. Synthetic quartz (for Si), rutile (Ti), corundum (Al), Cr_2O_3 (Cr), MnO (Mn), hematite (Fe), periclase (Mg), wollastonite (Ca), F-phlogopite (F) as well as natural albite (Na), adularia (K) and Cl-rich hastingsite (Cl) were used as standards. The Bence and Albee (1968) method was employed for matrix corrections. Detection limits for Cl and F were ~0.02 and 0.08 wt.% (3σ level), respectively.

Aspidolite and phlogopite

Point analyses in the mica grains were carefully selected on the basis of the back-scattered electron images. Chemical compositions of aspidolite and phlogopite are given in Table 1 and Fig. 3. Their chemical formulae were calculated on the basis of 11 O atoms. The total Fe was expressed as Fe^{2+}.

The Na content of aspidolite is between 0.67 and 0.96 a.p.f.u.; X_{Na} [= Na/(Na+K)] ranges from 0.67 to 0.95. The occupancy of the interlayer ranges from 0.94 to 1.03 a.p.f.u. In sharp contrast to the interlayer-deficient Na mica, wonesite [$Na_{0.5}\square_{0.5}Mg_{2.5}Al_{0.5}AlSi_3O_{10}(OH)_2$] (Rieder *et al*., 1998), the interlayer of aspidolite is almost fully occupied. The total number of octahedral cations is 2.93–3.00 a.p.f.u., a value close to the ideal number of 3 a.p.f.u. Compared to ideal aspidolite, aspidolite from Kasuga-mura is poorer in Si (2.52–2.62 a.p.f.u.), but correspondingly richer in tetrahedral Al (= ^{IV}Al; 1.38–1.48 a.p.f.u.). Si content exceeds 2.5 a.p.f.u., which marks the boundary between aspidolite [$NaMg_3AlSi_3O_{10}(OH)_2$] and preiswerkite [$NaMg_2AlAl_2Si_2O_{10}(OH)_2$]. $X_{Fe^{2+}}$ [= Fe^{2+}/(Fe^{2+}+Mg)] ranges from 0.08 to 0.10. The Ti content is always low (<0.05 a.p.f.u.). The Cl and F contents are $\leqslant$0.05 wt.% and $\leqslant$0.23 wt.%,

TABLE 1. Chemical composition (wt.%) of aspidolite and phlogopite.

	As	As	As	As	IPh	Phr
SiO_2	37.0	37.3	36.9	37.0	36.4	36.1
TiO_2	0.96	0.91	0.93	0.77	0.82	0.65
Al_2O_3	22.7	22.9	23.5	22.5	22.8	22.0
Cr_2O_3	n.d.	n.d.	n.d.	n.d.	n.d.	n.d.
FeO	4.12	4.11	4.07	4.13	4.03	5.74
MnO	n.d.	n.d.	0.07	0.06	n.d.	0.10
MgO	22.1	22.0	21.8	22.4	21.4	20.1
CaO	0.04	n.d.	0.04	n.d.	n.d.	0.12
Na_2O	6.79	6.74	6.64	5.94	2.32	0.96
K_2O	0.97	1.01	1.33	2.27	7.55	9.36
F	0.16	0.15	0.11	0.18	0.10	n.d.
Cl	n.d.	n.d.	n.d.	n.d.	n.d.	n.d.
−O=F+Cl	0.07	0.06	0.05	0.08	0.04	0.00
H_2O*	4.26	4.29	4.31	4.25	4.22	4.20
Total	99.0	99.4	99.7	99.4	99.6	99.3
Atomic proportions based on 11 O atoms						
Si	2.556	2.567	2.536	2.559	2.556	2.579
^{IV}Al	1.444	1.433	1.464	1.441	1.444	1.421
Total	4.000	4.000	4.000	4.000	4.000	4.000
^{VI}Al	0.404	0.424	0.440	0.393	0.443	0.432
Ti	0.050	0.047	0.048	0.040	0.043	0.035
Cr						
Fe^{2+}	0.238	0.237	0.234	0.239	0.237	0.343
Mn			0.004	0.004		0.006
Mg	2.276	2.257	2.234	2.310	2.240	2.141
Total	2.968	2.965	2.960	2.986	2.963	2.957
Ca	0.003		0.003			0.009
Na	0.910	0.899	0.885	0.797	0.316	0.133
K	0.085	0.089	0.117	0.200	0.676	0.853
Total	0.998	0.988	1.005	0.997	0.992	0.995
Total cations	7.966	7.953	7.965	7.983	7.955	7.952
F	0.035	0.033	0.024	0.039	0.022	
Cl						
OH	1.965	1.967	1.976	1.961	1.978	2.000
$X_{Fe^{2+}}$	0.095	0.095	0.095	0.094	0.096	0.138
X_{Na}	0.914	0.910	0.884	0.799	0.318	0.135

As = aspidolite, IPh = phlogopite interleaved with aspidolite, Phr = phlogopite rim, $X_{Fe^{2+}} = Fe^{2+}/(Fe^{2+}+Mg)$, $X_{Na} = Na/(Na+K)$, n.d. = not detected.
* H_2O calculation based on the assumption of OH+F+Cl = 2.0 a.p.f.u.

respectively. The wide range of ^{IV}Al (0.96−1.48 a.p.f.u.) in aspidolite in this study and in the literature as shown in Fig. 3 indicates that the tschermakite-type substitution ($^{VI}Mg^{IV}Si \rightarrow {}^{VI}Al^{IV}Al$) is the main factor controlling the aspidolite composition.

The phlogopite interleaved with aspidolite is remarkably variable in Na (0.07−0.48 a.p.f.u.); X_{Na} ranges from 0.07 to 0.48. The HRTEM study revealed that Na and K in this mica are resolved to a different interlayer region to form interstratified phlogopite and aspidolite at a monolayer

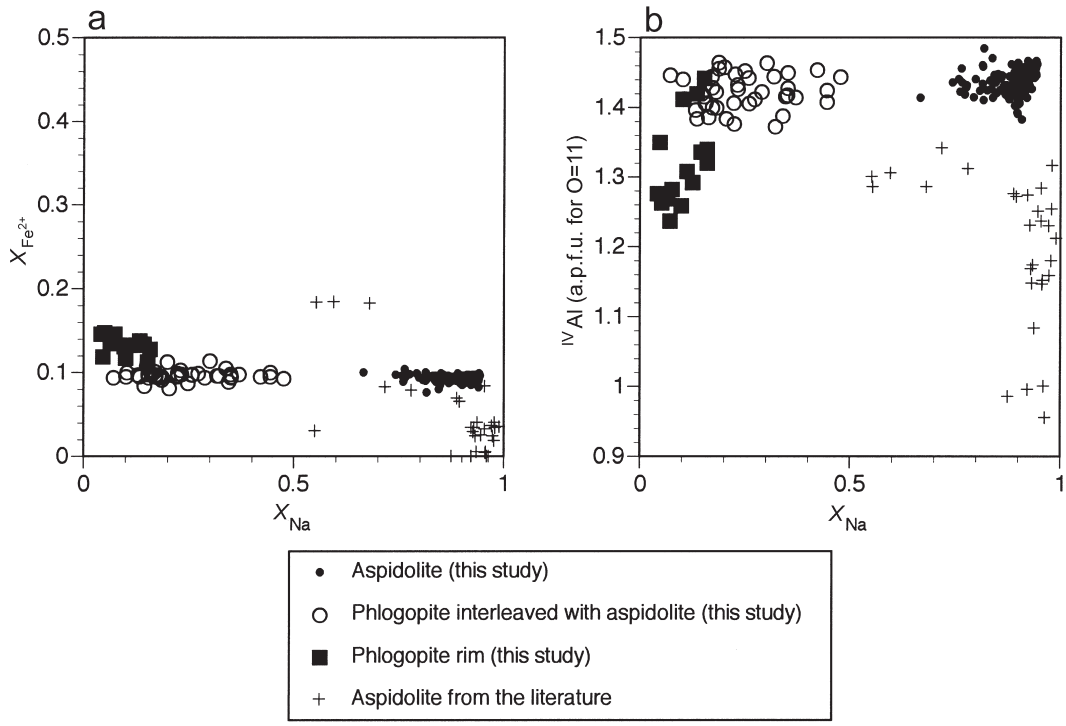

FIG. 3. (*a*) X_{Na}-$X_{Fe^{2+}}$ and (*b*) X_{Na}-^{IV}Al plots of aspidolite and phlogopite in this study. Plots of aspidolite from the literature are also shown. Data are from Arai *et al*. (1997), Augé (1987), Costa *et al*. (2001), Garnier *et al*. (2004), Lorand and Cottin (1987), Matsumoto and Arai (1997), Peng *et al*. (1995), Schiano *et al*. (1997), Schreyer *et al*. (1980), Talkington *et al*. (1986) and Tsujimori *et al*. (1998).

level (Kogure *et al*., 2004). This fluctuation of the Na-K ratio may be due to the fine interstratification of two micas on a nm scale, which hardly contributes to the contrast in the back-scattered images. The wide range of X_{Na} of the interleaved phlogopite may represent some analytical artifacts. However, the ranges of $X_{Fe^{2+}}$ (0.08–0.11) and ^{IV}Al (1.37–1.47 a.p.f.u.) of the interleaved phlogopite are almost constant irrespective of the variable X_{Na} ratios, and similar to those of aspidolite (Fig. 3). Therefore, these data are sufficient to indicate that the compositions of the tetrahedral and octahedral sites of the interleaved phlogopite are similar to those of aspidolite. The total numbers of octahedral and interlayer cations of the interleaved phlogopite are 2.92–2.98 and 0.95–1.03 a.p.f.u., respectively.

The phlogopite rim has higher $X_{Fe^{2+}}$ (0.11–0.15) and lower X_{Na} (0.04–0.16) and ^{IV}Al contents (1.24–1.44 a.p.f.u.) than the interleaved phlogopite (Fig. 3). Its totals of octahedral and interlayer cations are 2.91–2.96 and 0.99–1.03 a.p.f.u., respectively. Both types of phlogopite contain a small amount of Ti (<0.05 a.p.f.u.) and F (<0.35 wt.%). Chlorine contents in phlogopite are below the limit of detection.

Other minerals

The amphibole grains consist of an ^{IV}Al-poor core and ^{IV}Al-rich rim. The core is pargasite with ^{IV}Al of 2.08–2.19 a.p.f.u. (O = 23) and $X_{Fe^{2+}}$ of 0.13–0.16. The rim of amphibole is magnesio-sadanagaite with ^{IV}Al and $X_{Fe^{2+}}$ of 2.56–2.84 a.p.f.u. and 0.20–0.27, respectively. The rim is slightly more enriched in K (0.09–0.11 a.p.f.u.) than the core (0.04–0.05 a.p.f.u.). The representative formula of the rim is $(Na_{0.91}K_{0.09})_{\Sigma 1.00}(Ca_{1.95}Na_{0.03}Mn_{0.02})_{\Sigma 2.00}(Mg_{2.90}Al_{0.98}Fe^{2+}_{0.76}Ti_{0.30}Fe^{3+}_{0.06})_{\Sigma 5.00}(Si_{5.40}Al_{2.60})_{\Sigma 8.00}O_{22}(OH_{1.87}F_{0.13})_{\Sigma 2.00}$. A detailed discussion of the chemical composition of amphibole was given by Banno *et al*. (2004). The $X_{Fe^{2+}}$ value of chlorite is 0.12–0.29. Meionite

TABLE 2. Powder XRD data for a mica fragment consisting of aspidolite-1*M* and phlogopite-1*M*.

		Aspidolite-1*M*			Phlogopite-1*M*		
$I_{obs.}$	$d_{obs.}$	$d_{calc.}$*	*h k l*	$I_{calc.}$#	$d_{calc.}$**	*h k l*	$I_{calc.}$$
70	10.09				10.08	0 0 1	100
100	9.77	9.77	0 0 1	100			
3	5.05				5.04	0 0 2	2
5	4.91	4.89	0 0 2	<1			
25	4.59	4.58	0 2 0	17	4.60	0 2 0	9
20	4.54				4.55	1 1 0	11
15	4.46	4.46	1 1 0	30			
15	3.74	3.75	$\bar{1}$ 1 2	89			
15	3.66				3.66	$\bar{1}$ 1 2	36
15	3.40				3.40	0 2 2	46
30	3.36				3.36	0 0 3	41
15	3.33	3.34	0 2 2	69			
50	3.26	3.26	0 0 3	79			
6†	3.16				3.15	1 1 2	42
15	2.97	2.97	$\bar{1}$ 1 3	50			
		2.97	1 1 2	51			
15	2.93				2.92	$\bar{1}$ 1 3	29
100	2.61	2.62	$\bar{1}$ 3 1	90	2.61	$\bar{1}$ 3 1	59
		2.62	$\bar{1}$ 3 0	33	2.61	2 0 0	29
25	2.55	2.55	$\bar{2}$ 0 2	9			
		2.55	2 0 0	61			
10	2.50				2.50	1 3 1	3
					2.50	$\bar{2}$ 0 2	3
20	2.45	2.45	$\bar{1}$ 3 2	41			
40	2.43				2.43	$\bar{1}$ 3 2	21
					2.43	2 0 1	11
6	2.34	2.33	2 0 1	14			
8	2.29	2.29	0 4 0	4	2.30	0 4 0	3
		2.29	$\bar{2}$ 2 1	5	2.29	$\bar{2}$ 2 1	4
8	2.26				2.27	2 2 0	5
					2.26	$\bar{2}$ 0 3	2
					2.26	1 3 2	5
20	2.19	2.19	$\bar{1}$ 3 3	56			
		2.19	1 3 2	21			
25	2.17				2.17	$\bar{1}$ 3 3	30
					2.17	2 0 2	15
15	2.05	2.05	$\bar{2}$ 0 4	24			
		2.05	2 0 2	20			
6	2.02				2.02	0 0 5	12
15	2.00				2.00	$\bar{2}$ 0 4	8
					2.00	1 3 3	16
5	1.955	1.954	0 0 5	17			
10†	1.915	1.919	$\bar{1}$ 3 4	9	1.910	$\bar{1}$ 3 4	5
		1.920	1 3 3	9	1.910	2 0 3	2

* Calculated from refined cell parameters: a = 5.291(8), b = 9.16(2), c = 10.12(2) Å, β = 105.1(1)º.
** Calculated from refined cell parameters: a = 5.309(3), b = 9.194(5), c = 10.237(5) Å, β = 99.95(3)º.
# Calculated from assumed model of crystal structure (Kogure *et al*., 2004).
$ Calculated from crystal-structure refinement (Alietti *et al*., 1995).
† Estimated from data with the external Si standard.

molecules [100(Ca+Mg+Fe+Mn+Ti)/(Na+K+Ca+Mg+Fe+Mn+Ti)] make up 51–53% of scapolite. Titanite contains up to 1.49 wt.% Al_2O_3.

Physical and optical properties

Aspidolite is light brown in hand specimen and white in powdered form. It has perfect (001) cleavages, and its thin laminae are tough and elastic. Aspidolite does not expand in water. The Mohs hardness is <5½, probably 2–3 as estimated by the analogy with phlogopite. The density (calc.) is 2.885 g/cm^3. Aspidolite is optically biaxial negative with elongation positive and $Z \parallel$ cleavage. In thin section, it is pleochroic with X = colourless with yellowish tint and $Y = Z$ = pale yellowish brown.

X-ray diffraction study

Mica fragments, a few hundreds of μm long and <10 μm thick, were handpicked from the thin sections examined with back-scattered electron imaging. X-ray powder diffraction patterns of the mica fragments were obtained using a Gandolfi camera of 114.6 mm diameter employing Ni-filtered Cu-$K\alpha$ radiation. The complete diffraction pattern of a pure aspidolite, however, could not be obtained due to the presence of thin phlogopite layers intercalated with aspidolite. The data were recorded on an imaging plate and processed with a Fuji BAS-2500 bio-imaging analyser using a computer program written by Nakamuta (1999). Peak positions were determined by the profile-fitting method using a program developed by Nakamuta (1993). Observed d spacings were corrected by the Toraya (1993) method using an internal Si-standard (NBS, #640b). Indexing of the XRD patterns was based on the comparison with diffraction intensities calculated from the crystal parameters for aluminian phlogopite (Phl3a) of Alietti *et al*. (1995) and from assumed models of the crystal structure of aspidolite-1M and aspidolite-1A (Kogure *et al*., 2004). Aspidolite-1M is monoclinic, space group $C2/m$ and $Z = 2$; aspidolite-1A is triclinic, space group $C\bar{1}$ and $Z = 2$ (Kogure *et al*., 2004). The observed diffraction peaks shown in Tables 2 and 3 can be explained by a mixture of aspidolite-1M and phlogopite-1M, and of aspidolite-1A and phlogopite-1M, respectively. These two patterns are clearly different from each other in a range of lattice spacing between 2.75 and 4.46 Å. The d values of critical peaks are 4.46, 3.74 and 2.97 Å for aspidolite-1M, and 4.28, 4.01, 3.46, 3.11, 2.87 and 2.75 Å for aspidolite-1A. The refined unit-cell parameters are a = 5.291(8), b = 9.16(2), c = 10.12(2) Å, β = 105.1(1)º and V = 473(1) Å^3 for aspidolite-1M, and a = 5.289(6), b = 9.16(1), c = 9.892(9) Å, α = 94.45(9), β = 97.74(9), γ = 90.0(1)º and V = 473.4(9) Å^3 for aspidolite-1A.

The refined unit-cell parameters of phlogopite are also presented in Tables 2 and 3. Aspidolite has a distinctly smaller basal spacing than phlogopite due to the smaller ionic radius of Na relative to K. The decrease in the basal spacing is ~0.3 Å, which is almost the same as the difference in the spacing between paragonite and muscovite (Brigatti and Guggenheim, 2002). The length of the b axis for aspidolite is less than that for phlogopite (Tables 2 and 3). This shortening is probably also due to the K ⇌ Na substitution. However, the difference in the b length is ~0.4%, which is less than that (~1.2 %) between paragonite (Lin and Bailey, 1984) and muscovite (Güven, 1971). In dioctahedral micas, the ionic radius of K is too large for the cavity space in the tetrahedral sheet after full tetrahedral rotation has taken place, and thus incorporation of K into the dioctahedral micas causes a smaller ditrigonal rotation angle and greater b length (Bailey, 1984). On the contrary, phlogopite has a cavity space large enough to accommodate K, which is indicated by calculated K–O bond lengths for ideal trioctahedral biotite (Hewitt and Wones, 1975). The increase of the cavity space by incorporation of K in the dioctahedral micas can explain the smaller difference in the b length between aspidolite and phlogopite relative to that between paragonite and muscovite.

Formation of aspidolite-phlogopite

In the Kasuga sample, aspidolite is closely associated with the interleaved phlogopite. The P-T condition of the Kasuga-mura area is estimated at <2.5 kbar and <640ºC (Suzuki, 1975). The aspidolite and interleaved phlogopite are thought to be stable equilibrium phases under metamorphic conditions. The (001) plane-parallel alternation of aspidolite and phlogopite (Fig. 2) may be interpreted as reflecting a miscibility gap between these two phases as suggested by Schreyer *et al*. (1980) and Costa *et al*. (2001). Similar chemical compositions of the octahedral

TABLE 3. Powder XRD data for a mica fragment composed of aspidolite-1*A* and phlogopite-1*M*.

Aspidolite-1*A*					Phlogopite-1*M*		
$I_{obs.}$	$d_{obs.}$	$d_{calc.}$*	*h k l*	$I_{calc.}$#	$d_{calc.}$**	*h k l*	$I_{calc.}$$
50	10.07				10.08	0 0 1	100
80	9.73	9.77	0 0 1	100			
2	5.01				5.04	0 0 2	2
3	4.88	4.89	0 0 2	<1			
		4.57	0 2 0	14	4.60	0 2 0	9
40	4.57	4.57	$\bar{1}$ 1 0	5	4.55	1 1 0	11
		4.52	1 1 0	11			
6	4.39	4.37	1 1 $\bar{1}$	2	4.40	$\bar{1}$ 1 1	2
4	4.28	4.27	$\bar{1}$ 1 1	8			
		4.27	0 2 $\bar{1}$	9			
5	4.01	4.02	0 2 1	1			
		4.02	1 $\bar{1}$ 1	28			
8	3.93				3.93	1 1 1	17
15	3.66				3.66	$\bar{1}$ 1 2	36
8	3.62	3.61	1 1 $\bar{2}$	26			
10	3.46	3.48	$\bar{1}$ 1 2	11			
		3.47	0 2 $\bar{2}$	48			
15	3.40				3.40	0 2 2	46
30	3.36				3.36	0 0 3	41
40	3.26	3.26	0 0 3	79			
25†	3.15				3.15	1 1 2	42
10†	3.11	3.09	1 1 2	34			
15	2.92				2.92	$\bar{1}$ 1 3	29
6	2.87	2.86	1 1 $\bar{3}$	26			
3	2.75	2.76	$\bar{1}$ 1 3	23			
		2.76	0 2 $\bar{3}$	12			
3	2.72				2.71	0 2 3	15
		2.62	$\bar{2}$ 0 1	16	2.62	$\bar{1}$ 3 1	59
		2.62	1 3 $\bar{1}$	45	2.61	2 0 0	29
100	2.62	2.62	1 3 0	16			
		2.62	2 0 0	45			
		2.56	0 2 3	16			
		2.55	$\bar{1}$ 3 1	62			
30	2.55	2.56	1 $\bar{1}$ 3	4			
		2.55	1 $\bar{3}$ 1	9			
15	2.51				2.51	1 3 1	3
					2.50	$\bar{2}$ 0 2	3
		2.45	1 3 $\bar{2}$	21			
20	2.45	2.45	2 0 1	21			
					2.43	$\bar{1}$ 3 2	21
25	2.43				2.43	2 0 1	11
4	2.33	2.33	$\bar{1}$ 3 2	14			
		2.28	2 2 $\bar{1}$	4	2.30	0 4 0	3
6	2.29	2.28	0 4 0	3	2.29	$\bar{2}$ 2 1	4
		2.28	$\bar{2}$ 2 0	3			
		2.26	$\bar{2}$ 2 1	3	2.27	2 2 0	5
5	2.26	2.26	0 4 $\bar{1}$	2	2.26	$\bar{2}$ 0 3	2
		2.26	2 2 0	4	2.26	1 3 2	5

and tetrahedral layers between aspidolite and interleaved phlogopite (Fig. 3) seem to support this view. Aspidolite has a relatively large layer offset of ~0.9 Å (Kogure *et al*., 2004). This interlayer structure in aspidolite is distinctly different from that in phlogopite, which has a negligible amount of layer offset (Bailey, 1984), indicating that aspidolite is not simply the Na

TABLE 3. (*contd*.)

		Aspidolite-1*A*			Phlogopite-1*M*		
$I_{obs.}$	$d_{obs.}$	$d_{calc.}$*	*h k l*	$I_{calc.}$#	$d_{calc.}$**	*h k l*	$I_{calc.}$$
25	2.19	2.19	$\bar{2}$ 0 3	11			
		2.19	1 3 $\bar{3}$	28			
		2.19	1 3 2	11			
		2.19	2 0 2	28			
		2.19	2 2 $\bar{2}$	4			
		2.19	0 4 1	4			
25	2.17				2.17	$\bar{1}$ 3 3	30
					2.17	2 0 2	15
8	2.05	2.05	$\bar{1}$ 3 3	20			
		2.05	1 $\bar{3}$ 3	24			
10	2.02				2.02	0 0 5	12
10	1.994				1.995	$\bar{2}$ 0 4	8
					1.995	1 3 3	16
6	1.956	1.954	0 0 5	17			
10†	1.916	1.921	$\bar{2}$ 0 4	4	1.910	$\bar{1}$ 3 4	5
		1.921	1 3 $\bar{4}$	5	1.910	2 0 3	2
		1.919	1 3 3	4			
		1.919	2 0 3	4			

* Calculated from refined cell parameters: a = 5.289(6), b = 9.16(1), c = 9.892(9) Å, α = 94.45(9), β = 97.74(9), γ = 90.0(1)º.
** Calculated from refined cell parameters: a = 5.309(4), b = 9.201(9), c = 10.234(8) Å, β = 99.96(5)º.
# Calculated from assumed model of crystal structure (Kogure *et al*., 2004).
$ Calculated from crystal-structure refinement (Alietti *et al*., 1995).
† Estimated from data with the external Si standard.

analogue of phlogopite. This structural difference between aspidolite and phlogopite can explain the assumed miscibility gap between these two phases. Matsuda and Henmi (1986) synthesized the mica minerals in the compositional join between phlogopite and aspidolite at 1 kbar and 550ºC, and found an incomplete solid solution between the two micas for compositions having X_{Na} that ranges from 0 to 0.65. The unpublished hydrothermal ion-exchange experiments of Liu (1989) indicated a miscibility gap between aspidolite and phlogopite at 2 kbar and 700ºC for compositions with X_{Na} of 0.4–0.7. These experimental results support evidence for the existence of a solvus between aspidolite and phlogopite.

On the contrary, the phlogopite rim forms thin films which surround the aspidolite interleaved with phlogopite (Fig. 2). The phlogopite rim is interpreted as a later product, which may have formed by the interaction between the aspidolite interleaved with phlogopite and a K-rich fluid. The phlogopite rim has greater $X_{Fe^{2+}}$ and smaller X_{Na} and ^{IV}Al than the interleaved phlogopite (Fig. 3). These distinct chemical compositions suggest different conditions of formation for the two types of phlogopite. The zonal structure of amphibole with increasing K from the core to the rim also supports this view. In addition, Suzuki (1975) studied the metasomatic bands and veins (e.g. biotite-plagioclase rock) developed in the contact aureole in Kasuga-mura and concluded that these rocks formed by interaction between basic hornfels and K-rich fluids from granite at a later stage of metamorphism. This K metasomatisum is also consistent with our interpretation concerning the formation of the phlogopite rim.

The hydration properties of aspidolite were reported by Carman (1974) and Franz and Althaus (1976). Carman (1974) showed that at low temperature, synthetic aspidolite and water-rich vapour react to form hydrated aspidolite. The aspidolite from Kasuga-mura is invariably coated by rims of phlogopite (Fig. 2). These rims may have prevented the retrogressive hydration of aspidolite, as discussed by Schreyer *et al*. (1980).

Acknowledgements

We thank Dr Y. Okuyama of AIST and Prof. M. Enami of Nagoya University for their critical and thoughtful comments on an earlier version of this manuscript. Constructive reviews by Dr H.-J. Förster and Prof. W. Schreyer improved the manuscript.

References

Alietti, E., Brigatti, M.F. and Poppi, L. (1995) The crystal structure and chemistry of high-aluminium phlogopite. *Mineralogical Magazine*, **59**, 149–157.

Arai, S., Matsukage, K., Isobe, E. and Vysotskiy, S. (1997) Concentration of incompatible elements in oceanic mantle: effect of melt/wall interaction in stagnant or failed melt conduits within peridotite. *Geochimica et Cosmochimica Acta*, **61**, 671–675.

Augé, T. (1987) Chromite deposits in the northern Oman ophiolite: mineralogical constraints. *Mineralium Deposita*, **22**, 1–10.

Bailey, S.W. (1984) Crystal chemistry of the true micas. Pp. 13–60 in: *Micas* (S.W. Bailey, editor). Reviews in Mineralogy, **13**, Mineralogical Society of America, Washington, D.C.

Banno, Y., Miyawaki, R., Matsubara, S., Makino, K., Bunno, M., Yamada, S. and Kamiya, T. (2004) Magnesiosadanagaite, a new member of the amphibole group from Kasuga-mura, Gifu Prefecture, central Japan. *European Journal of Mineralogy*, **16**, 177–183.

Bence, A.E. and Albee, A.L. (1968) Empirical correction factors for the electron microanalysis of silicates and oxides. *Journal of Geology*, **76**, 382–403.

Brigatti, M.F. and Guggenheim, S. (2002) Mica crystal chemistry and the influence of pressure, temperature, and solid solution on atomistic models. Pp. 1–98 in: *Micas: Crystal Chemistry and Metamorphic Petrology* (A. Mottana, F.P. Sassi, J.B. Thompson, Jr. and S. Guggenheim, editors). Reviews in Mineralogy and Geochemistry, **46**, Mineralogical Society of America, and the Geochemical Society, Washington, D.C.

Carman, J.H. (1974) Synthetic sodium phlogopite and its two hydrates: stabilities, properties, and mineralogic implications. *American Mineralogist*, **59**, 261–273.

Costa, F., Dungan, M.A. and Singer, B.S. (2001) Magmatic Na-rich phlogopite in a suite of gabbroic crustal xenoliths from Volcán San Pedro, Chilean Andes: Evidence for a solvus relation between phlogopite and aspidolite. *American Mineralogist*, **86**, 29–35.

Franz, G. and Althaus, E. (1976) Experimental investigation on the formation of solid solutions in sodium-aluminum-magnesium micas. *Neues Jahrbuch für Mineralogie Abhandlungen*, **126**, 233–253.

Garnier, V., Ohnenstetter, D. and Giuliani, G. (2004) L'aspidolite fluorée: rôle des évaporates dans la genèse du rubis des marbres des Nangimali (Azad-Kashmir, Pakistan). *Comptes Rendus Geoscience*, **336**, 1245–1253.

Güven, N. (1971) The crystal structure of $2M_1$ phengite and $2M_1$ muscovite. *Zeitschrift für Kristallographie*, **134**, 196–212.

Hewitt, D.A. and Wones, D.R. (1975) Physical properties of some synthetic Fe-Mg-Al trioctahedral biotites. *American Mineralogist*, **60**, 854–862.

Kogure, T., Banno, Y. and Miyawaki, R. (2004) Interlayer structure in aspidolite, the Na analogue of phlogopite. *European Journal of Mineralogy*, **16**, 891–897.

Lin, C.-Y. and Bailey, S.W. (1984) The crystal structure of paragonite-$2M_1$. *American Mineralogist*, **69**, 122–127.

[Liu, X.F. (1989) Signification pétrogénétique des micas trioctaédriques sodiques. Modélisation expérimentale dans le système Na_2O-K_2O-MgO-Al_2O_3-SiO_2-H_2O-(TiO_2-HF-D_2O). Thèse de Doctorat; Université d'Orléans, 87pp.] cited in Costa, F., Dungan, M.A. and Singer, B.S. (2001) Magmatic Na-rich phlogopite in a suite of gabbroic crustal xenoliths from Volcán San Pedro, Chilean Andes: Evidence for a solvus relation between phlogopite and aspidolite. *American Mineralogist*, **86**, 29–35.

Lorand, J.P. and Cottin, J.Y. (1987) Na- Ti- Zr- H_2O-rich mineral inclusions indicating postcumulus chrome-spinel dissolution and recrystallization in the Western Laouni mafic intrusion, Algeria. *Contributions to Mineralogy and Petrology*, **97**, 251–263.

Matsuda, T. and Henmi, K. (1986) Syntheses of trioctahedral micas in the compositional join phlogopite–sodium phlogopite. *Journal of the Mineralogical Society of Japan*, special issue, **17**, 187–193 (in Japanese with English abstract).

Matsumoto, I. and Arai, S. (1997) Characterization of chromian spinel as a tool of petrological exploration for podiform chromitite. *Resource Geology*, **47**, 189–199.

Nakamuta, Y. (1993) The determination of lattice parameters of a small crystal with a Gandolfi camera. *Journal of the Mineralogical Society of Japan*, **22**, 113–122 (in Japanese with English abstract).

Nakamuta, Y. (1999) Precise analysis of a very small mineral by an X-ray diffraction method. *Journal of the Mineralogical Society of Japan*, **28**, 117–121 (in Japanese with English abstract).

Peng, G., Lewis, J., Lipin, B., McGee, J., Bao, P. and Wang, X. (1995) Inclusions of phlogopite and

phlogopite hydrates in chromite from the Hongguleleng ophiolite in Xinjiang, northwest China. *American Mineralogist*, **80**, 1307–1316.

Rieder, M., Cavazzini, G., D'yakonov, Yu.S., Frank-Kamenetskii, V.A., Gottardi, G., Guggenheim, S., Koval', P.V., Müller, G., Neiva, A.M.R., Radoslowich, E.W., Robert, J.-L., Sassi, F.P., Takeda, H., Weiss, Z. and Wones, D.R. (1998) Nomenclature of the micas. *The Canadian Mineralogist*, **36**, 905–912.

Schiano, P., Clocchiatti, R., Lorand, J.P., Massare, D., Deloule, E. and Chaussidon, M. (1997) Primitive basaltic melts included on podiform chromites from the Oman Ophiolite. *Earth and Planetary Science Letters*, **146**, 489–497.

Schreyer, W., Abraham, K. and Kulke, H. (1980) Natural sodium phlogopite coexisting with potassium phlogopite and sodian aluminian talc in a metamorphic evaporite sequence from Derrag, Tell Atlas, Algeria. *Contributions to Mineralogy and Petrology*, **74**, 223–233.

Suzuki, K. (1975) On some unusual bands and veins metasomatically developed in the contact aureole in Kasuga-mura, Gifu-ken. *Journal of the Geological Society of Japan*, **81**, 487–504 (in Japanese with English abstract).

Suzuki, K. (1977) Local equilibrium during the contact metamorphism of siliceous dolomites in Kasuga-mura, Gifu-ken, Japan. *Contributions to Mineralogy and Petrology*, **61**, 79–89.

Talkington, R.W., Watkinson, D.H., Whittaker, P.J. and Jones, P.C. (1986) Platinum group element-bearing minerals and other solid inclusions in chromite of mafic and ultramafic complexes: chemical compositions and comparisons. Pp. 223–249 in: *Metallogeny of Basic and Ultrabasic Rocks (Regional Presentations)* (B. Carter, M.K.R. Chowdhury, S. Janković, A.A. Marakushev, L. Morten, V.V. Onikhimovsky, G. Raade, G. Rocci and S.S. Augustithis, editors). Theophrastus, Athens, Greece.

Toraya, H. (1993) The determination of unit-cell parameters from Bragg reflection data using a standard reference material but without a calibration curve. *Journal of Applied Crystallography*, **26**, 583–590.

Tsujimori, T., Saito, D., Ishiwatari, A., Miyashita, S. and Sokolov, S.D. (1998) Electron microprobe element image of zoned chromian spinel with hydrous mineral inclusions in a chromitite from Elistratova ophiolite, Far East Russia. *Science Reports of the Kanazawa University*, **43**, 1–11.

von Kobell, F. (1869) Über den Aspidolith, ein Glied aus der Biotit- und Phlogopit-Gruppe. *Sitzungsberichte der Königl. Bayerischen Akademie der Wissenschaften zu München*, Jg. 1869, **1**, 364–366.

[*Manuscript received 7 May 2005: revised 14 September 2005*]